TRANSPORT
ISSN 1648-4142 / eISSN 1648-3480
2015 Volume 30(2): 129–134
doi:10.3846/16484142.2013.816364

3D FINITE ELEMENT MODELING OF SLING WIRE ROPE IN LIFTING AND TRANSPORT PROCESSES

Gordana Kastratović, Nenad Vidanović

Faculty of Transport and Traffic Engineering, University of Belgrade, Belgrade, Serbia

Submitted 24 June 2011; accepted 13 January 2012;
first published online 16 October 2013

Abstract. Paper explores some aspects of 3D modeling of 'aircraft cable' as mostly used sling wire rope. First, the 1×19 stainless steel core of 'aircraft cable' was investigated. The analysis was carried out by finite element method based computer program. The software used allowed two different types of contacts, including friction. The sling wire rope core was subjected to two different types of axial loading. The obtained results were compared with the solutions calculated from the literature (Costello 2012). Finally, using the advanced modeling techniques, the parametric 3D model of 7×19 'aircraft cable' was analyzed using finite element method, in order to provide a better understanding and, hence, prediction, of the mechanical behavior of the sling wire ropes in lifting processes.

Keywords: 3D modeling; sling wire rope; axial loading; finite element method; lifting processes.

Introduction

'Aircraft cable' has become an accepted industry term for small diameter 7×7 and 7×19 construction wire rope intended for industrial and marine application. 'Aircraft cable' combines high strength with good fatigue resistance. Despite of the term 'Aircraft cable' these commercial grade cables are not approved to be used in any aircraft or similar applications. Other applications are too many to list but include control cables, strength members, stage rigging, suspension, lifting, transport, pulling applications and wire rope slings (Fig. 1).

The ability to handle materials, to move them from one location to another, whether during transport or at the worksite, is vital to all segments of industry. Various types of equipment have been designed specifically to aid in the movement of materials, machinery, etc. They include: cranes, derricks, hoists, powered industrial trucks, and conveyors. All these transport devices rely upon slings to hold their suspended loads. Slings are the most commonly used piece of materials-handling and lifting apparatus.

Wire rope slings are a basic material handling tool and are the most frequently used type of sling in industry today. They offer a strong, dependable, durable and economical option for most lifting applications. Their popularity is enhanced by the numerous sling configurations (Fig. 2) available to support a broad range of applications. These configurations include single and multipart slings, grommets, single leg slings, multiple leg bridles, and a wide variety of fittings and attachments.

Fig. 1. Sling wire rope application in lifting and transport processes

Corresponding author: Gordana Kastratović
E-mail: *g.kastratovic@sf.bg.ac.rs*

Taylor & Francis
Taylor & Francis Group

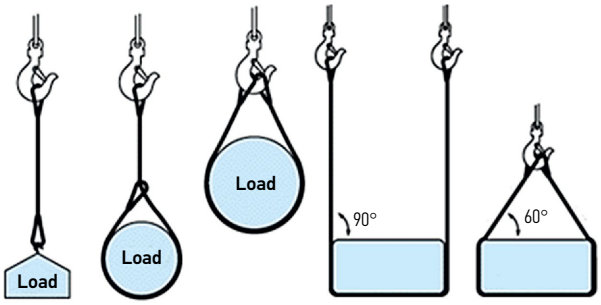

Fig. 2. Wire rope slings

Wire ropes are very important tensile structural members. It is well known that a major advantage of such elements is their capacity to support large axial load. They participate as one of crucial members of the dynamic model of a hoisting mechanism during the lifting operation (Bogdevičius, Vika 2005).

In order to predict the wire rope behavior, hence sling wire rope behavior, several theoretical models and analytical studies have been presented in the literature (Love 2011; Costello 2012). Most of them neglect frictional and contact effects, but there are some, that take those effects into consideration.

As technology and computer sciences were developing and became more available, numerical analyses started to be frequently used in predicting the wire rope behavior. The use of these analyses came as a need, because it was often required to conduct various tests during exploitation to evaluate wire rope structural condition and bearing capacity and to detect damage resulting from the repeated working load. Knowing that experimental work on wire rope requires specific, large and expensive testing devices, numerical analysis such as finite element analysis, as non-distractive method, was the logical next step in the wire rope behavior studies.

One of the first finite element analyses of simple straight strand has been presented by Jiang *et al.* (2000). Elata *et al.* (2004) developed a new model for simulating the mechanical response of an independ wire rope core (IWRC). Elastoplastic contact problem of laying wire rope using finite element analysis has been investigated by Sun *et al.* (2005).

A realistic 3D structural model and finite element analysis of a simple wire strand has been briefly explained by Erdönmez and İmrak (2009). The same authors presented 3D solid model and wire-by-wire analysis of IWRC (İmrak, Erdönmez 2010) and the frictionless contact effects in wire rope strand subjected to axial loading was analyzed.

Some of the mentioned analyses ignored frictional effects, but there were some (Jiang *et al.* 2000; Elata *et al.* 2004; Sun *et al.* 2005; Erdönmez, İmrak 2009; İmrak, Erdönmez 2010; Kastratović, Vidanović 2010), that took those effects into consideration. However, analysis of other contact effects in three layered ropes was neglected in available literature. Also, all of them introduced axial loading as applied axial strain, except in next work (Kastratović, Vidanović 2011) were authors used axial force which was evenly distributed between wires.

Because of these reasons and its complex geometry, it is still very difficult to model and analyze wire ropes, using numerical methods, such as finite element method. Also, this kind of analysis requires substantial computer resources. Nevertheless, numerical analysis must be employed to provide a better understanding, and hence prediction, of the mechanical behavior of the wire rope strands, thus reducing the need for expensive tests (because of which the experimental results reported in the literature are very limited). In order to accomplish all of that, the aim of this paper was to explore some aspects of 3D modeling of a sling wire rope using the finite element method based computer program with special emphasis on different types of contacts and different types of axial loading.

1. Finite Element Model and Analysis

Model of the wire rope considered here is shown in Figs 3 and 4. As it can be seen, the 1×19 wire rope was investigated. It is a stainless steel core of a 7×19 stainless steel wire rope. The 7×19 strand stainless steel wire rope is extremely flexible because of its strength and high corrosion resistant qualities. It is used in general engineering applications, especially stainless steel wire rope slings.

The 3D finite element model of the 1×19 wire rope was created (Fig. 5). First, the parametric geometrical model was created by using CAD commercial software. The obtained geometrical model was then imported to

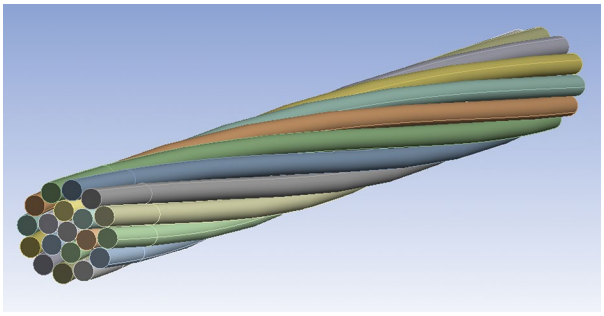

Fig. 3. 1×19 stainless steel core

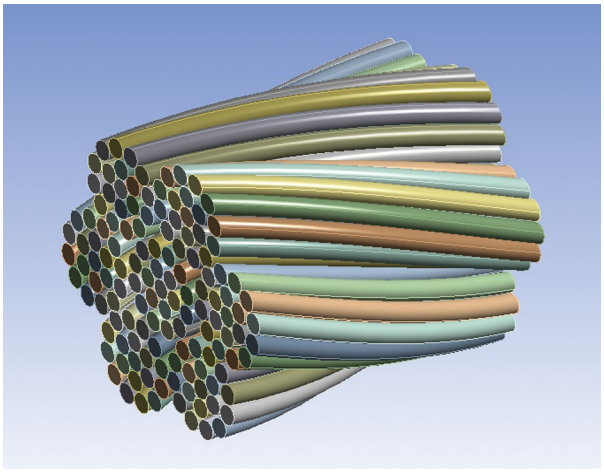

Fig. 4. 7×19 stainless steel wire rope

the finite element based computer program. This program allowed specification of material properties, generation of finite element mesh, application of loads, and contact definition as well as solving and obtaining necessary output data.

It is well known that very important issue in any finite element analysis is the element selection and mesh size. If the created mesh is too coarse then the problem may not converge due to increased time steps and there will be no solution. On the other hand, too fine mesh may cause similar difficulty because of the large number of elements and nodes, i.e. large numbers of equations. This can also significantly increase computational time.

So, 3D models were made with optimum numbers of elements (Figs 5 and 6). The goal of meshing in used software was to provide robust, easy to use meshing tools that will simplify the mesh generation process. These tools have the benefit of being highly automated along with having a moderate to high degree of user control. Here we used mesh sweeping method which is default for solid bodies. The body can be meshed very efficiently with hexahedral and wedge elements using this technique. The number of nodes and elements for a swept body is usually much smaller than ones meshed with other methods. In addition, less time is required to create these elements.

Finite element used for meshing all analyzed models was a brick solid element that is used in 3D modeling

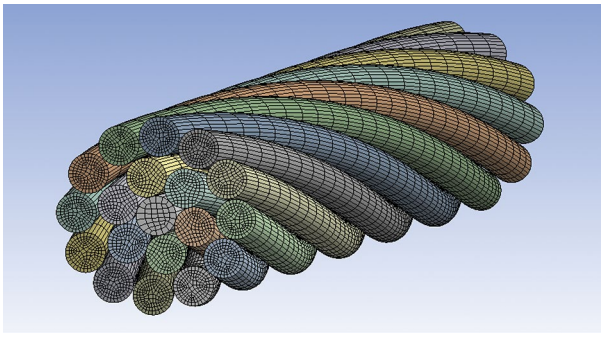

Fig. 5. 3D finite element model of the 1×19 wire rope core

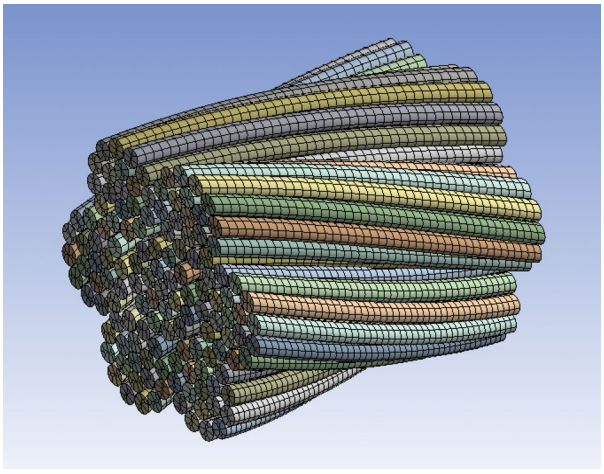

Fig. 6. 3D finite element model of the 7×19 wire rope

of solid structures, as default element. The same kind of element was used in research by İmrak and Erdönmez (2010), but in different software. It is a higher order 3D 20-nodes solid element that exhibits quadratic displacement behavior. The element is defined by 20-nodes having three degrees of freedom per node: translations in the nodal *X*, *Y*, and *Z* directions. The element supports plasticity, hyperelasticity, creep, stress stiffening, large deflection, and large strain capabilities. It also has mixed formulation capability for simulating deformations of nearly incompressible elastoplastic materials, and fully incompressible hyperelastic materials.

This type of element is well suited to modeling irregular meshes (such as those produced by various CAD/CAM systems), which was the case here.

Another important issue for this particular problem represents the contacts between wires and friction. Regardless of friction, contacts between wires exist and must be taken into consideration. They determine how the wires can move relative to one another and the distribution of load between them, as well, even when the friction is neglected.

In this analysis two types of contacts were applied. Bonded contact is a linear type of contact. It is the default configuration of contact and applies to all contact regions (surfaces, solids, lines, faces, edges). If contact regions are bonded, then no sliding or separation between faces or edges is allowed, as if the bodies were glued.

Also, frictional contact was available, and this nonlinear analysis was carried out, as well. In this setting, two contacting faces can carry shear stresses up to a certain magnitude across their interface before they start sliding relative to each other. It only applies to regions of faces. This state is known as 'sticking'. The model defines an equivalent shear stress at which sliding on the face begins as a fraction of the contact pressure. Once the shear stress is exceeded, the two faces will slide relative to each other. The coefficient of friction can be any non-negative value.

As it can be seen on Figs 1 and 2 the main loading of sling wire rope is the axial loading. Since the single leg sling is the most frequently used, the model of 7×19 'aircraft cable' as the wire rope that is suitable for that kind of sling was analyzed in this paper.

The analysis was first carried out for the 1×19 stainless steel core of the 7×19 'aircraft cable'. The wire rope core is a member of complex wire ropes that carries the greatest amount of axial loading.

2. Finite Element Analysis (FEA) of 1×19 Wire Rope Core

The axial loading behavior was analyzed, with two different load settings.

2.1. Axial Loading by Applying Evenly Distributed Axial Force

First, axial loading behavior was investigated by applying an axial force to the free end of the 1×19 stainless steel core, while the other end was fixed. The total force of 10 000 N was applied in increments of 2000 N. The total force was evenly distributed between wires.

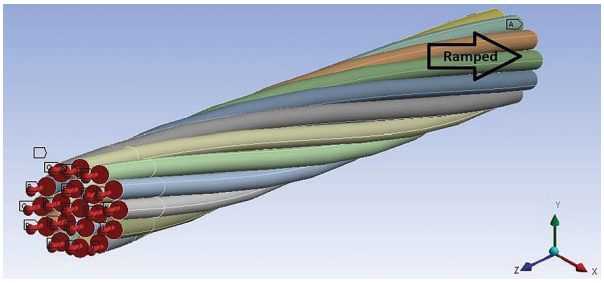

Fig. 7. Boundary conditions for 1×19 wire rope core

All the wires in the analyzed stainless steel core have the same radius r = 0.335 mm, with the inner pitch length of 44 mm and the outer pitch length of 87.983 mm. The overall length of the wire rope model was 44 mm.

The model was meshed, and the prescribed boundary conditions (Fig. 7) were used for solving: on one end of the model the degrees of freedom in all three directions were constrained, and on the other end the displacement in x and y directions were restrained to zero.

The linear contact elastic behavior was analyzed, were the modulus of elasticity was $E = 1.88 \cdot 10^{11}$ Pa, and was Poisson's ratio $\nu = 0.3$.

For model with frictional contact, nonlinear analysis was carried out. The additional material properties used in elastic-plastic analysis are defined as: the yield strength $R_{p0.2} = 1.54 \cdot 10^9$ Pa, tangent modulus $E_t = 2.46 \cdot 10^{10}$ Pa, ultimate tensile strength $R_m = 1.8 \cdot 10^9$ Pa, while the friction coefficient was $\mu = 0.115$. The material properties are obtained from paper by İmrak and Erdönmez (2010).

The solutions were obtained for 329 088 numbers of nodes or 73 120 elements, for both linear and nonlinear contact settings. This number of nodes was selected because it provided the best balance between calculation accuracy and calculation time, which can be significant and requires substantial computer resources.

The solution calculated in this analysis was total deformation. The maximum deformation, i.e., strain occurs on the outer wires.

As it can be seen on the previous diagram (Fig. 8), there is practically no difference between results obtained for different types of contacts. Also, the diagram shows excellent agreements between obtained results and with the results calculated by Costello (2012) linearized theory. It is, also, obvious that the analyzed model exhibits elastic behavior.

Besides the resulting axial strain, the equivalent stresses (von Mises) were calculated as well. The variation of those stresses throughout the model can be seen in previous figures (Figs 9 and 10), for bonded and frictional contact settings, respectively. Better distribution of stresses exhibits the nonlinear model, because of the friction.

We would like to emphasize that the main results of the analyses that were carried out in this paper are shown on the diagrams on the Figs 8 and 11. The equivalent stresses, shown on Figs 9 and 10, were calculated

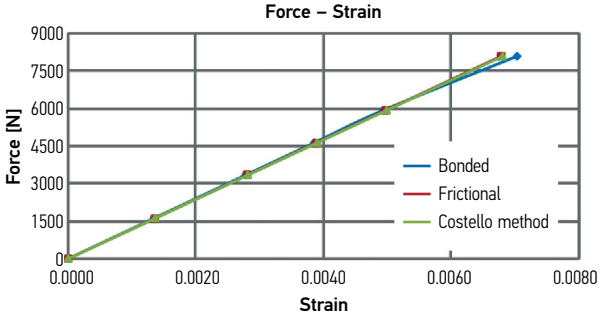

Fig. 8. Diagram of resulting axial strain for 1×19 wire rope core

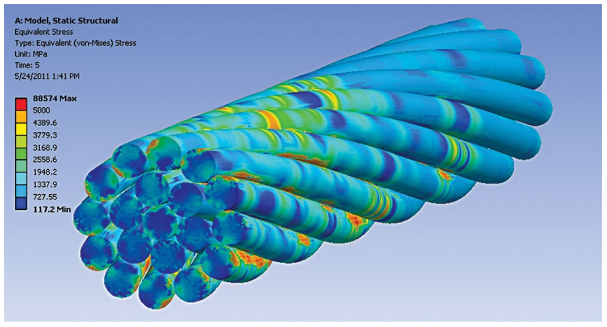

Fig. 9. Von Mises stresses for bonded contact settings – linear case solution for 1×19 wire rope core

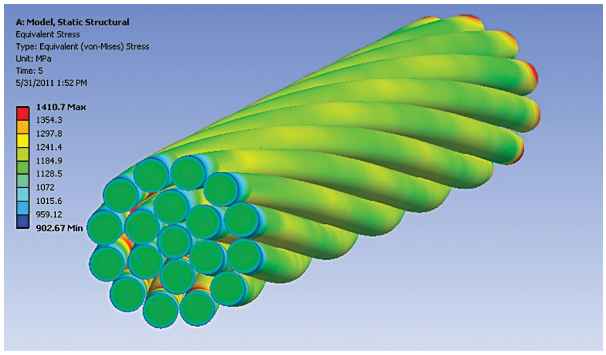

Fig. 10. Von Mises stresses for frictional contact settings – nonlinear case solution for 1×19 wire rope core

in order to show distribution of loads. The accuracy of calculated values is poor, because the number of finite elements used is small for this kind the analysis. This is one of the well-known setbacks of finite elements analysis. As it was mentioned before, this number of elements was selected because it provided the best balance between calculation accuracy of the main results (the resulting force reaction in the case of axial strain loading and total deformation in case of evenly distributed axial force loading) and calculation time.

2.2. Axial Loading by Applying Axial Strain

Also, axial loading behavior was investigated by applying an axial strain to the free end of the 1×19 stainless steel core, with the 5 corresponding increments, while the other end of the model was fixed.

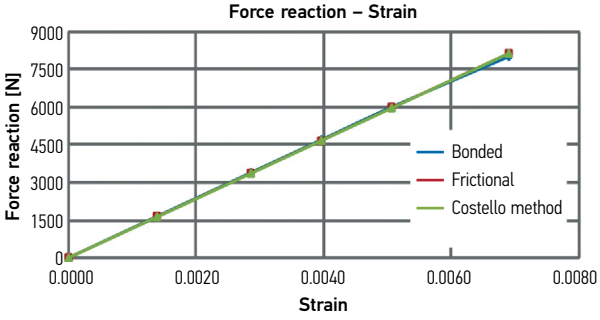

Fig. 11. Diagram of resulting force reaction for 1×19 wire rope core

The other applied settings for linear contact, and nonlinear frictional contact were the same as in the previous analysis.

The output data in this load case were total force reaction, which was calculated as sum of all reaction forces of the individual wires.

Like in previous load case, the diagram (Fig. 11) shows excellent agreements between obtained results and with the results calculated by Costello (2012) linearized theory.

Besides the resulting force reaction, the equivalent stresses (von Mises) were calculated as well. The variation of those stresses throughout the model can be seen in previous figures (Figs 12 and 13), for bonded and frictional contact settings, respectively. As it can be seen, in this load case, also, better distribution of stresses exhibits the nonlinear model, because of the friction.

The remark about equivalent stresses is the same as in the previous case.

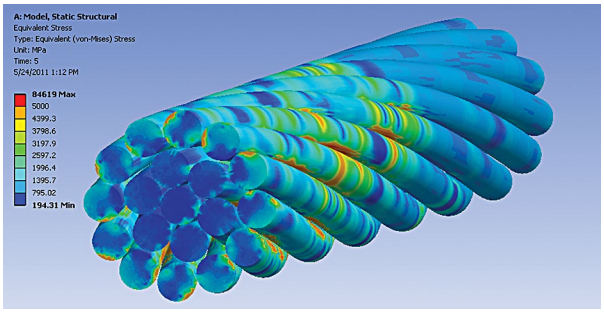

Fig. 12. Von Mises stresses for bonded contact settings – linear case solution for 1×19 wire rope core

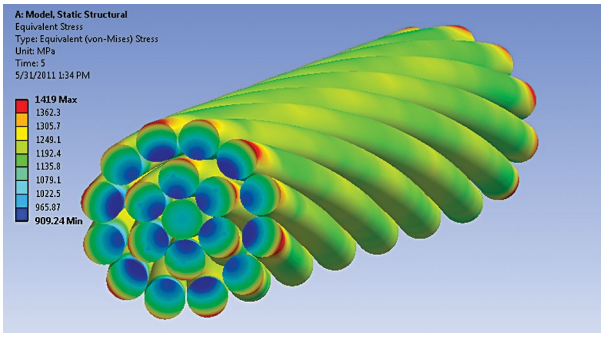

Fig. 13. Von Mises stresses for frictional contact settings – nonlinear case solution for 1×19 wire rope core

3. FEA of 7x19 Wire Rope

Finally, the model of 7×19 strand stainless steel wire rope was investigated. As it was mentioned earlier, it is extremely flexible because of its strength and high corrosion resistant qualities, and it is often used as sling wire rope.

Axial loading behavior was investigated by applying an axial strain to the free end of the wire rope, with the 5 increments, in accordance with the previous analyses. The other end of the model was fixed (Fig. 14).

All the wires in the analyzed wire rope have the same radius $r = 0.335$ mm, with the inner pitch length of 44 mm and the outer pitch length of 87.983 mm, while the outer strand pitch length was 66 mm. The number of contacts in this case was 342, which was almost five times greater than for the 1×19 steel core. This increased the complexity of the calculation enormously. So, the overall length of the wire model in this case was 11 mm.

This was, also, the reason why the solutions were obtained for 304 839 numbers of nodes or 55 116 elements, for both linear and nonlinear contact settings, which was less than in the previous case. However, this number of nodes was selected because it provided the best balance between calculation accuracy and calculation time.

On the diagram shown on Fig. 15, the obtained results are compared with the ones calculated by Costello linearized theory. As it can be seen, there is discrepancy between them. This can be assigned to the fact that the Costello's (2012) method was carried out on the assumption that there were no contacts between wires, except in the radial direction.

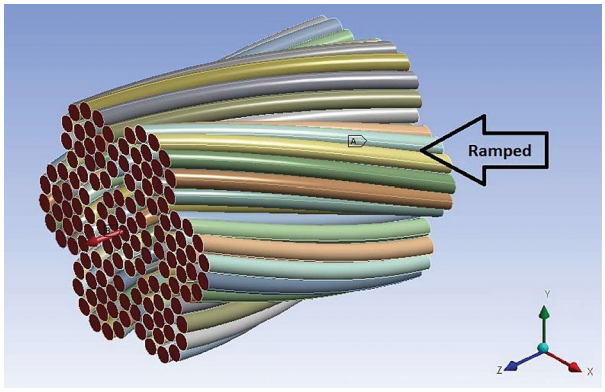

Fig. 14. Boundary conditions for 7×19 wire rope

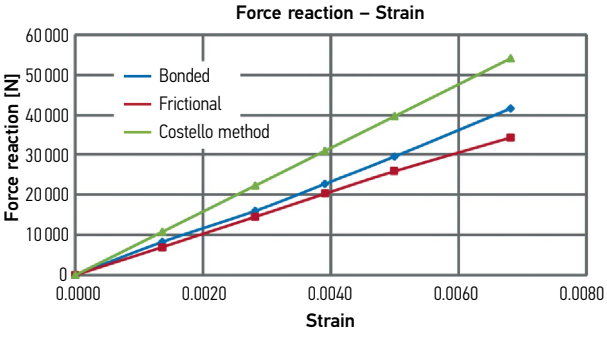

Fig. 15. Diagram of resulting force reaction for 7×19 wire rope

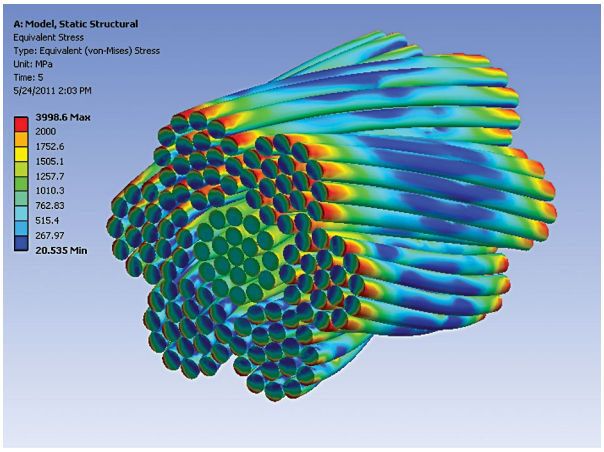

Fig 16. Von Mises stresses for bonded contact settings – linear case solution for 7×19 wire rope

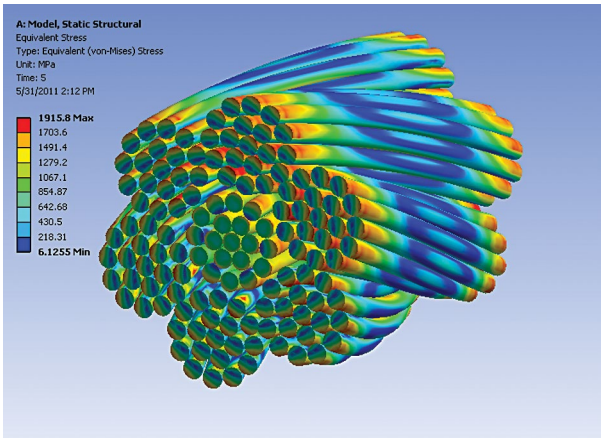

Fig 17. Von Mises stresses for frictional contact settings – nonlinear case solution for 7×19 wire rope

Besides the resulting force reaction, the equivalent stresses (von Mises) were calculated as well. The variation of those stresses throughout the model can be seen in next figures (Figs 16 and 17), for bonded and frictional contact settings, respectively.

As it can be seen, better distribution of stresses exhibits the nonlinear model, because of the friction, which is the case in real exploitation conditions. The remark about equivalent stresses is the same as in previous cases.

Conclusions

Using commercial software, which is currently widely available, some aspects of 3D modeling of an aircraft cable were investigated, which are widely used as wire rope slings.

The investigation was carried out by the finite element method. The sling wire rope core, as a member of complex wire ropes that carries the greatest amount of axial loading, was subjected to two different types of axial loading.

The two different types of contacts between wires were applied, including frictional contact. It is established that the obtained results showed excellent agreements with the results from the literature that was available.

Finally, the analysis was carried out on the model of 7×19 sling wire rope, also for linear and nonlinear contact, but only for one load setting. In this case, when the load was applied as axial strain, there was considerable difference between results (Fig. 15). This emphasizes, once more, the significance of creating the suitable finite element model of the wire rope, in order to provide a better understanding and, hence prediction, of the mechanical behavior of the sling wire rope in lifting and transport processes.

Acknowledgements

The authors wish to express the gratitude to Ministry of Science of Republic of Serbia, for supporting their current research through projects TR 33036.

References

Bogdevičius, M.; Vika, A. 2005. Investigation of the dynamics of an overhead crane lifting process in a vertical plane, *Transport* 20(5): 176–180.

Costello, G. A. 2012. *Theory of Wire Rope*. 2nd edition. Springer. 138 p.

Elata, D.; Eshkenazy, R.; Weiss, M. P. 2004. The mechanical behavior of a wire rope with an independent wire rope core, *International Journal of Solids and Structures* 41(5–6): 1157–1172. http://dx.doi.org/10.1016/j.ijsolstr.2003.11.021

Erdönmez, C.; İmrak, C. E. 2009. Modeling and numerical analysis of the wire strand, *Journal of Naval Science and Engineering* 5(1): 30–38.

İmrak, C. E.; Erdönmez, C. 2010. On the problem of wire rope model generation with axial loading, *Mathematical and Computational Application* 15(2): 259–268.

Jiang, W. G.; Henshall, J. L.; Walton, J. M. 2000. A concise finite element model for three-layered straight wire rope strand, *International Journal of Mechanical Sciences* 42(1): 63–86. http://dx.doi.org/10.1016/S0020-7403(98)00111-8

Kastratović, G.; Vidanović, N. 2010. The analysis of frictionless contact effects in wire rope strand using the finite element method, *Transport & Logistics* 19: 33–40.

Kastratović, G. M.; Vidanović, N. D. 2011. Some aspects of 3D finite element modeling of independent wire rope core, *FME Transactions* 39(1): 37–40.

Love, A. E. H. 2011. *A Treatise on the Mathematical Theory of Elasticity*. 4th edition. Dover Publications. 672 p.

Sun, J.-F.; Wang, G.-L.; Zhang, H.-O. 2005. Elasto-plastic contact problem of laying wire rope using FE analysis, *The International Journal of Advanced Manufacturing Technology* 26(1–2): 17–22. http://dx.doi.org/10.1007/s00170-004-2120-9